The changes in La Niña induced summertime interannual variability of sea level anomaly along the western boundary of the Bay of Bengal

Arnab Mukherjee[1] · Supriyo Ghosh[1,2]

Abstract

In this study, interannual variability and associated dynamics of sea level anomaly (SLA) along the western boundary of the Bay of Bengal (WBoB) during the summer (June–September) seasons of La Niña years between 1998–2016 has been investigated using satellite observations and a linear, continuously stratified (LCS) model. To quantify interannual variability along WBoB, regions have been divided into three parts, which include northern (NBoB), central (CBoB), and southern (SBoB). Satellite observation shows negative interannual SLA at all three regions of WBoB during summertime La Niña years of 1998, 1999, and 2007, which became positive during summertime La Niña years of 2010, 2011 and 2016. The LCS model simulates reasonably well the observed interannual SLA variability along WBoB, depending on the forcing mechanisms and La Niña episode. Using dedicated boundary experiments on the LCS model, it has been observed that interannual variability of SLA during summertime La Niña events are significantly dominated by remote forcing from Equatorial Indian Ocean (EIO) and interior BoB. The maximum dominant forcing for negative interannual SLA during summertime La Niña years of 1998 and 2007 originates from the EIO. However, negative interannual SLA during summertime La Niña year of 1999 is mostly dominated by interannual SLA forced by interior BoB. LCS model also shows that positive interannual SLA during summertime La Niña years of 2010, 2011, and 2016 are significantly dominated by remote forcing from both interior BoB and EIO via constructive interference.

Keywords Satellite altimeter · Interannual sea level anomaly · Western boundary of Bay of Bengal · Linear wind driven model, La Niña

1 Introduction

The ongoing global sea level rise, which is mainly forced by anthropogenic global warming, implies the importance of knowing the mechanisms behind its interannual variability since it may exacerbate sea level rise threats (Church and White 2011; Hu and Bates 2018). Global sea level rise is a significant concern for the people residing in coastal cities around the globe. North Indian Ocean (NIO) is divided into two major basins, known as the Bay of Bengal (BoB) and the Arabian Sea AS). Coastal Upwelling or downwelling along the western boundary of the BoB (WBoB) is mainly dominated by seasonally reversing monsoon winds (Shetye et al. 1991, 1996; Shankar et al. 2002). During summertime (June–August), sea level variability along WBoB is dominated by north-eastward propagated winds and are responsible for coastal upwelling (Shetye et al. 1991). Similarly, wind direction changes southwestward during winter and is responsible for coastal downwelling along WBoB (Shetye et al. 1996).

Observed study of interannual variability of sea level anomaly (SLA) started in the 1990's. Clarke and Liu (1994) showed using monthly tide gauge observations that interannual variability of SLA is mostly dominated by remote propagation of equatorial Kelvin and Rossby waves originated in the equatorial Indian Ocean. Changes in SLA interannual variability along WBoB are associated with changes in equatorial wind forcing, which is attributed to El Niño - Southern Oscillation (ENSO) (Rao et al. 2002; Srinivas et al. 2005; Jensen 2007; Aparna et al. 2012; Mukherjee

✉ Arnab Mukherjee
arnab@ncpor.res.in

1 ESSO-National Centre for Polar and Ocean Research (NCPOR), Ministry of Earth Sciences (MoES), Vasco Da Gama, Goa, India

2 Barcelona Super-computing Center, Barcelona, Spain

and Kalita 2019). Apart from ENSO, interannual sea level variability along WBoB is also influenced by the Indian Ocean Dipole (IOD) (Saji et al. 1999; Han and Webster 2002; Rao et al. 2002, 2009). Another study based on a satellite altimeter observed SLA along selected tracks of WBoB also showed the dominance of ENSO events on interannual SLA variability (Durand et al. 2009).

Using a wind-driven linear, continuously stratified (LCS) model, McCreary (1981); Han and Webster (2002); Aparna et al. (2012) showed that dynamics of interannual variability of the sea level along WBoB is linear and mostly dominated by remotely forced equatorial Indian Ocean (EIO) wind and interior BoB pumping. Previous studies also showed that SLA is negative during positive IOD and El Niño events, where it is positive during negative IOD and La Niña events with significant variations in their seasonal strengths (Srinivas et al. 2005; Aparna et al. 2012; Sreenivas et al. 2012; Mukherejee and Kalita 2019). Also, it has been observed that there is a distinction in the impact of ENSO and IOD on interannual SLA variability along WBoB (Aparna et al. 2012).

During positive IOD events, a peak of negative interannual SLA has been observed along WBoB from September to November (Aparna et al. 2012). However, during El Niño events, two peaks of negative SLA have been observed during both the summer and winter. A previous study also found that during only IOD events, interannual SLA variability along WBoB is significantly dominated by remote forcing from both EIO and interior BoB. However, during only El Niño events, the role of remote forcing from interior BoB is weak compared to forcing from EIO (Aparna et al. 2012). They also showed that interannual SLAs are weak and negligible during both La Niña and negative IOD years in the summer and winter seasons. During spring, the interannual variability of SLA is much weaker compared to both summer and winter seasons (Aparna et al. 2012; Mukherejee and Kalita 2019).

It is known from previous research that interannual SLA variability along WBoB is mostly dominated by ENSO and IOD events, but their study were limited only on the impact of the above events. No study has been performed on changes of their impacts during different years and if any other oceanic process is responsible for the modulation of interannual SLA variability along WBoB. In this study, a wind-driven LCS model has been used to study the dynamics of interannual SLA variability during La Niña years summertime along WBoB. Several others have used the LCS model to study the dynamics of SLA along WBoB at various time scales ranging from intraseasonal, seasonal, and interannual (Shankar et al. 1996; McCreary et al. 1996; Shankar et al. 2010; Suresh et al. 2013; Chatterjee et al. 2017; Mukherejee et al. 2017).

This manuscript presents a detailed analysis of summertime interannual SLA variability in the BoB. It is well known that during the above season, the strong monsoon winds and ENSO onset are expected to be the main SLA drivers along WBoB (Shankar et al. 2002; Schott et al. 2009). The impact of local (along WBoB) and remote (eastern boundary, equatorial Indian Ocean, and interior BoB) wind are estimated here. The detailed analysis of the study is restricted based on summertime La Niña episodes between 1998–2016.

The manuscript has been organized as follows. In Section 2, satellite altimeter observations, ocean model, numerical experiments and validation of the LCS model has been described. Observed and model simulated interannual variability of SLA in the BoB are described in Section 3. Linear dynamics related to interannual variability of SLA along WBoB has been described in Section 4. Section 5 concludes the manuscript with an overview and discussion.

2 Datasets and methodology

2.1 satellite datasets

In this study, a satellite altimeter derived gridded SLA data of daily temporal resolution were used. The horizontal resolution of the altimeter data is 0.25° X 0.25° in longitude–latitude directions. The satellite data has been downloaded from 01 January 1993 to April 2018 for detailed analysis in the manuscript. Recent updated (version 2021) satellite altimeter data has been downloaded from https://cds.climate.copernicus.eu/cdsapp#!/dataset/satellite-sea-level-global?tab=form. Twenty years (1998-2017) long-term mean has been removed from the data to quantify observed SLA. The altimeter SLA downloaded from the above reference is based on two satellite products. One satellite works as a reference and ensures long-term stability of the data. Another satellite product is used to improve accuracy, mesoscale processes, etc. The above reference data also have been used previously by several others in the Bay of Bengal (Srinivas et al. 2005; Durand et al. 2009; Aparna et al. 2012).

2.2 Ocean model

A linear, continuously stratified (LCS) model has been used (McCreary 1980, 1981) in this work to study the main drivers of interannual SLA along WBoB. A similar long-term mean has been removed from the sea level data using the LCS model to quantify observed SLA. LCS is a simple wind-driven model. The vertical solution of the model is based on the sum of 10 normal modes. Estimation of normal modes are based on density profile of Moore and McCreary (1990) and the detailed formulation of the LCS model related to normal vertical mode has been discussed in McCreary et al. (1996); Mukherejee et al. (2017). LCS model domain includes Indian ocean regions ranging from 30°E–120°E and 30°S–30°N
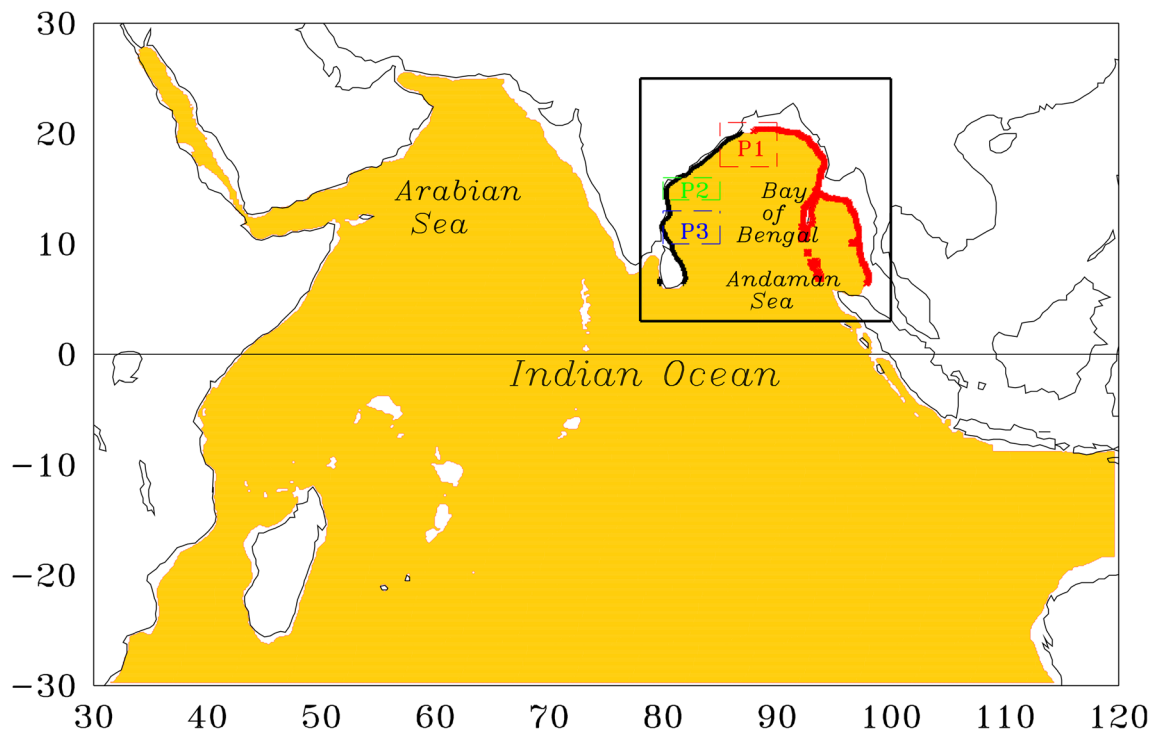
Fig. 1 The domain of the LCS model is shown here. A square box in solid black lines shows the region of interest in the Bay of Bengal (BoB). Yellow (white) colour shade shows ocean (land) mask with values of 1 (0). The solid red curve lines along the eastern and northern boundary of the BoB, including Andaman and Nicobar Islands, denotes the stretch of the coast along which the modified boundary condition (MBC) has been applied for LCS$_{EB}$. The black curve along the western boundary of the BoB (WBoB) denotes the stretch of the coast, in which MBC has been applied for LCS$_{WB}$. Dash rectangular boxes (P1, P2 and P3) in red, green, and blue color regions represents Northern BoB (NBoB; 85°E–90°EE, 17°N-21°N), Central BoB (CBoB; 80°E–85°E, 14°N–16°N) and Southern BoB (SBoB; 80°E–85°E, 10°N-13°N) respectively

(Fig. 1). The horizontal resolution of the model is set to 0.1° x 0.1° in longitude–latitude directions. Due to the linearity of the model, both nonlinear horizontal and vertical advection terms have been removed from the model equations. Also, base on previous model studies, it is known that the dynamics of interannual SLA along WBoB is mostly linear (Shankar et al. 2010; Aparna et al. 2012). It can be assumed that the absence of nonlinear terms in the LCS model equations will not have any major impact on the interannual summertime SLA along WBoB. The horizontal mixing of the model is based on the second-order linear Laplacian operator with a coefficient of 5 x 10^6 cm^2 s^{-1}. No slip-closed boundary condition has been used in the model.

Land-sea masking of the model is estimated using the topography of modified Etopo2 (Sindhu et al. 2007) for Indian Ocean. Continental shelf regions have been removed from the model by removing regions with a water depth of less than 200 m (Fig. 1). Narrow passages between Indian and Sri Lanka have been removed due to their shallow water depth. Also, Pacific Ocean masks have been removed from the model domain.

The model is forced using daily Tropflux (Praveen et al. 2013) wind stress from 01 January 1990 with an integration time of 15 seconds. Tropflux wind stress is available from January 1979 with a horizontal resolution of 1° x 1° in X–Y directions. The model has been initialized from the state of rest. The wind forcing switches to daily satellite observed scatterometer derived QuikSCAT (horizontal resolution of 0.5° x 0.5 ° in X–Y directions) and ASCAT (horizontal resolution of 0.25° x 0.25° in X–Y directions) from January 2000 and 2009 year respectively. LCS model simulation was performed from 01 January 1990 to 30 April 2018. This study uses model outputs from January 1998 to December 2016 for detailed analysis, including six La Niña summer seasons of 1998, 1999, 2007, 2010, 2011, and 2016.

2.3 Numerical experiments

The control run simulations using LCS are named LCSCR, based on wind forcing, as discussed above. Three additional numerical simulations have been performed using special boundary conditions and linear damper as discussed in McCreary et al. (1996); Chatterjee et al. (2017); Mukherejee et al. (2017); Mukherejee and Kalita (2019). One numerical experiment is related to the absence of WBoB local

Table 1 Detailed list of numerical experiments used in the manuscript to understand linear wind driven forcing mechanism using LCS model. Detailed configuration of the LCS model has been discussed in section 2

Experiment name	Detailed description of experiments model
LCS$_{WB}$	LCSCR-LCSCR with MBC along WBoB
LCS$_{EIO}$	LCSCR-LCSCR with linear damper along EIO
LCS$_{EB}$	LCSCR-LCSCR model with MBC along EBoB
LCS$_{BI}$	LCSCR- LCS$_{WB}$ - LCS$_{EIO}$ - LCS$_{EB}$

wind stress, which has been performed by allowing coastal Ekman flow to pass through the boundary. To achieve the above numerical experiments, no-slip boundary condition ($u_n=v_n=0$) has been modified. The modified boundary condition (MBC) is below as per McCreary et al. (1993).

$$\tilde{u}_n = \mathbf{n}.\mathbf{v_n} = -\mathbf{n}.\mathbf{k} \times \frac{\mathbf{F_n}}{f}; \tag{1a}$$

$$\tilde{v}_n = \mathbf{k} \times \mathbf{n}.\mathbf{v_n} = 0. \tag{1b}$$

In Equation (1a) and Equation (1b), **n** is the unit vector normal to the boundary, $\mathbf{F_n}$ is the wind-stress vector, **k** is the unit vector directed upward, f is the Coriolis frequency, $\tilde{u}_n$ and $\tilde{v}_n$ are velocity components perpendicular and parallel to the boundary. In one experiment, the above MBC has been applied along WBoB with ranging from 6.5°N to 20°N. First special boundary simulation has been named as LCS$_{WB}$ after subtracting the above special experiment solutions with LCSCR to isolate the forcing response only due to local wind along WBoB (Fig. 1). Similarly, for the second simulation, MBC has been applied along the eastern and northern boundaries of the BoB including Andaman and Nicobar islands (EBoB) and named it as LCS$_{EB}$, which represents the forcing response only due to the above remote coastal winds (Fig. 1). Above two numerical experiments related to the model also has been described in Table 1.

For another set of experiments, a linear damper between 6.5°N to 6.5°S has been used in the eastern EIO (east of 90°E) to stop equatorial wave response to BoB. The damping coefficient values have fixed to 1 at 6.5°N and 6.5°S.
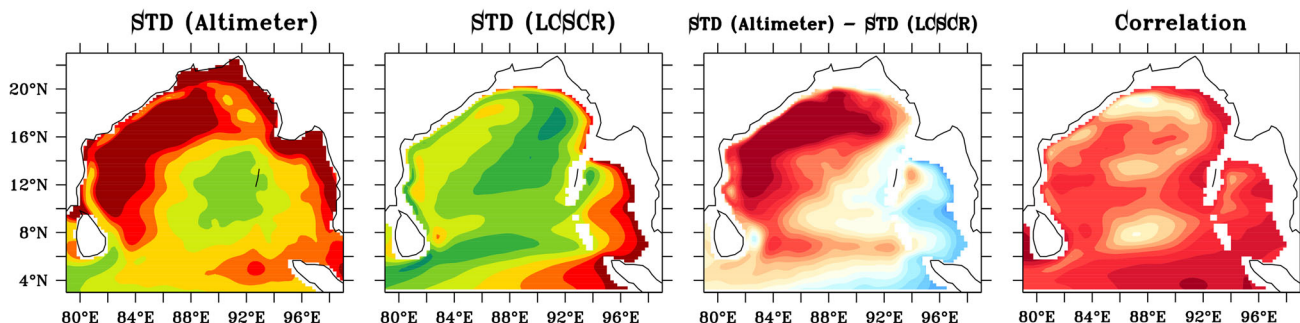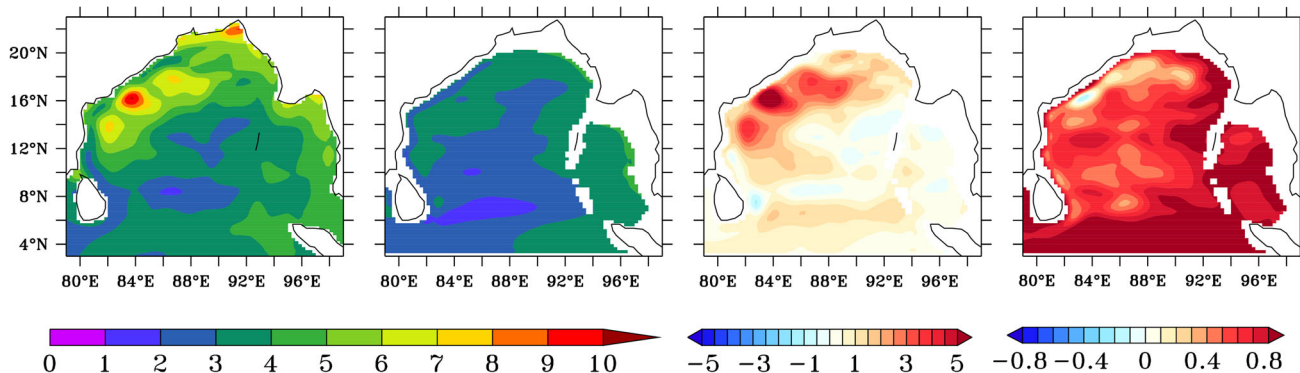
Fig. 2 The first row of the top panel shows standard deviations (STD in cm) of SLA at BoB using altimeter observations, the second row shows STD (in cm) of SLA using LCSCR, the third row shows the difference of STD (in cm) between the altimeter and LCSCR, and the last row shows the correlation (R) of SLA between altimeter and LCSCR. The bottom panel shows a similar analysis as the top panel, but for the inter-annual variability of the SLA by applying 400 days low-pass time series filter as discussed in section 2. Detailed statistics have been performed using data from 01 January 1998 to December 2016 for both altimeter and LCSCR

Table 2 Classification of La Niña years based on https://ggweather.com/enso/oni.htm between 1998 to 2016

| Name of	years
climate modes	(June – August)
Strong La Niña (SL)	1998, 1999, 2007 and 2010
Moderate La Niña (ML)	2011
Weak La Niña (WL)	2000, 2005, 2008 and 2016

Third simulation, named as LCS$_{EIO}$, has been estimated after subtracting the above experiment solutions with LCSCR to

isolate the forcing response only due to EIO. In the end, after subtracting all three numerical simulations (LCS$_{WB}$, LCS$_{EB}$ and LCS$_{EIO}$) with LCSCR, the response from the interior, BoB is quantified and named as LCS$_{BI}$. Please see Table 1 for a detailed list of numerical experiments using the LCS model.

2.4 Validation

A detailed validation of the LCS model from seasonal to interannual timescale was discussed in Shankar et al. (2010);
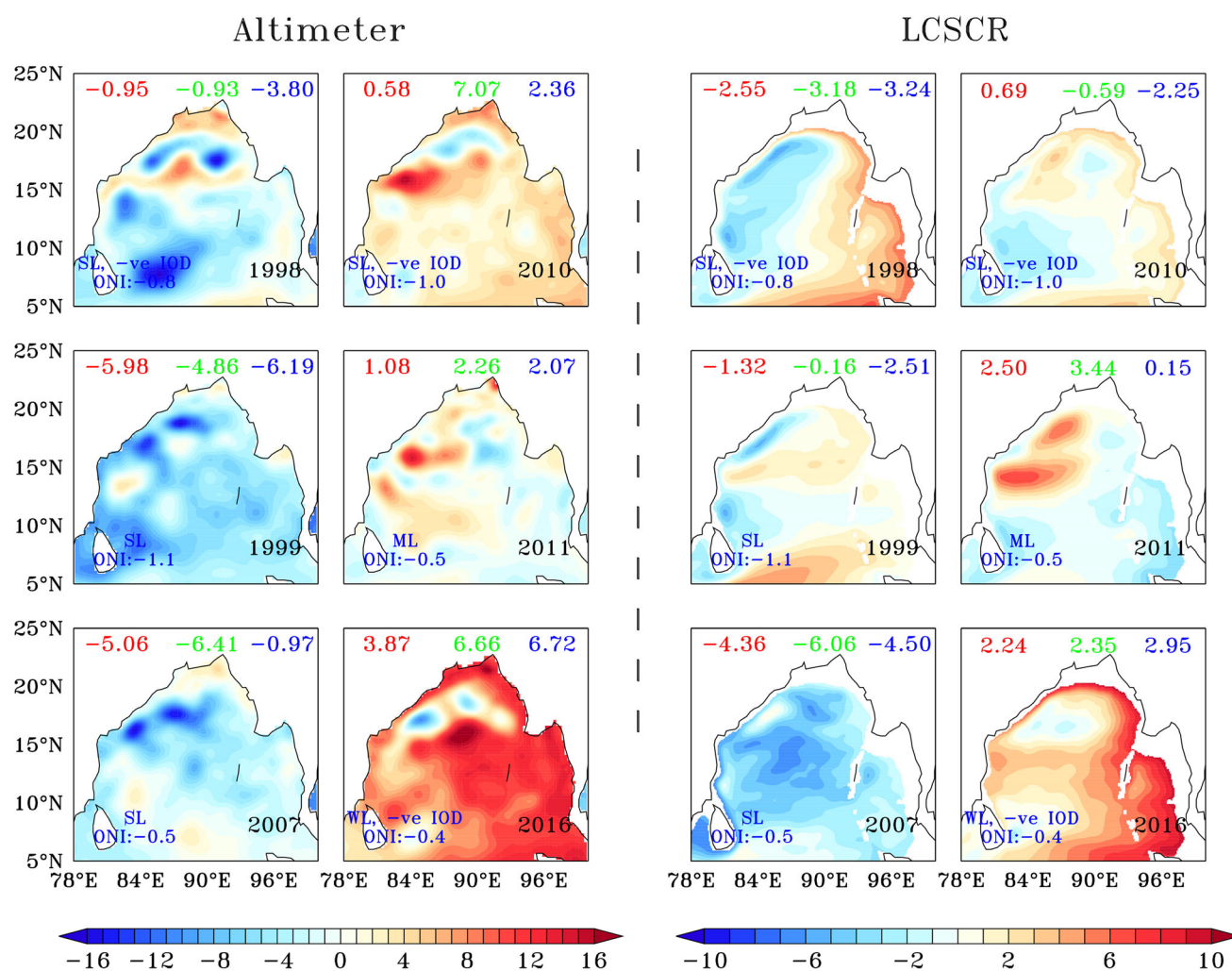
Fig. 3 The first and second column of the figure shows the altimeter observed interannual SLA (cm) at BoB during summer seasons La Niña years of 1998, 1999, 2007, 2010, 2011, and 2016 respectively. The third and fourth column of the figure shows LCSCR simulated interannual SLA (cm) at BoB during summertime of the above years. Values written in each box using red, green, and blue colours represent average val-

ues of interannual SLA for NBoB, CBoB, and SBoB regions as shown in Fig. 1. The difference in interannual SLA between the altimeter and LCSCR for the above six years is shown in Figure S1. The values of Oceanic Niño Index (ONI) written in each box has taken from https://ggweather.com/enso/oni.htm
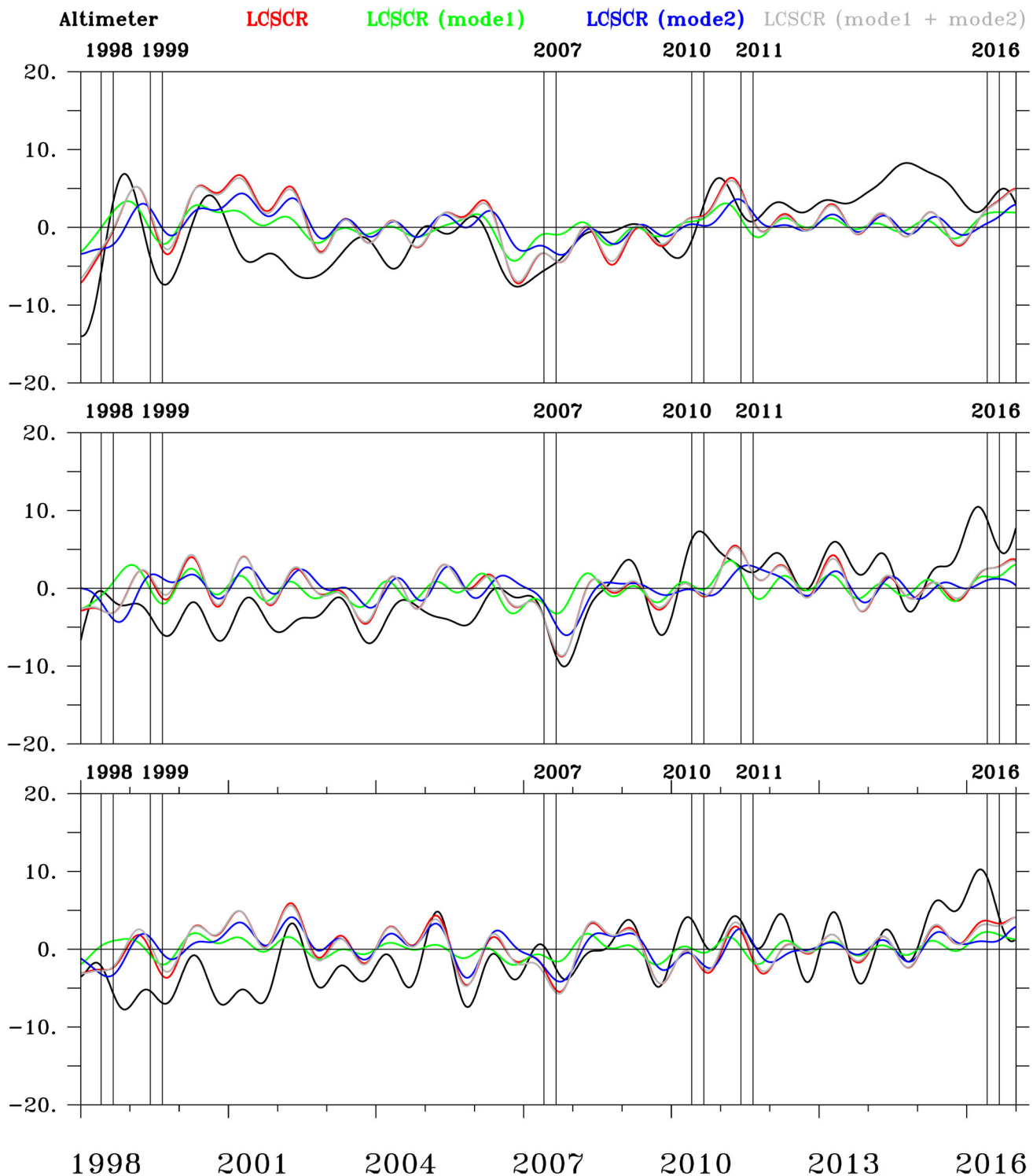
Fig. 4 The top panel of the figure shows the average interannual SLA for NBoB. The middle and bottom panel of the figure shows the average interannual SLA for CBoB and SBoB, respectively. In each panel, black, red, green, blue, and grey denote the altimeter, LCSCR, mode 1 of LCSCR, mode 2 of LCSCR, and the sum of LCSCR's first two modes, respectively. Summer seasons (June–August) of 1998, 1999, 2007, 2010, 2011, and 2016 have been shown in each panel using black boxes. Regions of averaging for NBoB, CBoB, and SBoB have been shown in Fig. 1. The structure of the vertical mode and density profile used in the LCSCR is shown in Figure S2

Aparna et al. (2012); Mukherejee et al. (2017); Mukherejee and Kalita (2019). For brevity, in this manuscript, statistical validation of LCSCR in the simulation of altimeter-observed interannual SLA in the BoB has been described (Fig. 2). To quantify the interannual variability of SLA, the seasonal variability has been removed using ~400 days low-pass time series $4'th$ order Butterworth filter (Duchon 1979). So, variability associated with less than annual time scale (~400 days) has been removed by applying the above filter. Also, during the estimation of statistical validation, SLA using LCSCR has been changed from the model grid to the altimeter grid.

It has been observed that the performance of LCSCR has improved in the simulation of the altimeter observed interannual SLA along WBoB compared to unfiltered SLA, which includes variability from intraseasonal to the seasonal and interannual time scale (Fig. 2). LCSCR shows a weak standard deviations (STD) compared to the altimeter for both unfiltered and interannual SLA in the BoB. As an example, high difference values (more than 6 cm) have been observed for the comparison of STD between SLA values of unfiltered altimeter and LCSCR. However, for interannual SLA, the difference in STD has been reduced to 2–3 cm. Similarly, an improved correlation (R) has been observed in the performance of LCSCR in the simulation of the altimeter observed interannual SLA in the entire BoB compared to unfiltered SLA (Fig. 2). Along WBoB, high values of R (more than 0.5) has been observed for interannual SLA using LCSCR with more than 90% statistical significance.

Observed data also show strong interannual variability of SLA with higher values of STD along WBoB compared to other parts of BoB, which includes central and eastern (Fig. 2). Substantial interannual variability of SLA along WBoB also has been observed using LCSCR. This further implies the strong dominance of Ekman Pumping-induced coastal upwelling/downwelling in the BoB.

2.5 Error range estimation

To estimate the Range of Errors (RE) associated with mean values of SLA, error values have been calculated for both model and observations using the equations below

$$RE = \sqrt{\frac{\sum_{n=1}^{N}(X_n - \overline{X})^2}{N(N-1)}}. \tag{1c}$$

in Eq. 1c, X_n is the nth reading in the data sets, $\overline{X}$ is the mean of the data sets, and N is the number of elements in the data sets. For this study, N values have been fixed to 7305 (20 years of data from 01 January 1997 to 31 December 2016).

3 Interannual SLA variability along WBoB during La Niña summer seasons

This section discusses the altimeter observed, and the LCSCR model simulated interannual SLA variability during summertime La Niña years between 1998–2016 along WBoB. Also, the estimation of the summer season is based on its average between June–August.

To describe the interannual variability of SLA along WBoB, regions have been divided into three boxes, which includes northern BoB (NBoB; 85°E–90°E, 17°N–21°N), central BoB (CBoB, 80°E-85°E, 14°N–16°N) and southern BoB (SBoB, 80°E–85°E, 10°N–13°N). All three above regions are shown in Fig. 1. La Niña events between 1998–2016 has been classified into three categories; Strong La Niña (SL), Moderate La Niña (ML) and Weak La Niña (WL) and years associated with the above events are shown in Table 2. Six summer seasons La Niña years of 1998 (SL), 1999 (SL), 2007 (SL), 2010 (SL), 2011 (ML) and 2016 (WL) has been used in this study which covers four strong, one moderate, and one weak La Niña events.

Observed data shows a strong presence of interannual variability during summertime La Niña years of 1998, 1999, 2007, 2010, 2011, and 2016 in the entire BoB (Fig. 3 and Fig. 4). Negative interannual SLA has been observed along WBoB during summertime La Niña years of 1998, 1999, and 2007. However, observed SLA shows positive interannual SLA along WBoB during the summer season La Niña year of 2010, 2011, and 2016 respectively. This later result implies that there is a strong presence of interannual variability associated with the impact of La Niña along WBoB. Also, it has been observed that there is a dominance of negative interannual SLA during La Niña years between 1998–2007 and positive interannual SLA between 2008–2016.

Model LCSCR reasonably well simulates above observed interannual variability of SLA along WBoB during summer seasons La Niña years between 1998–2016 (Fig. 3). As an example, an altimeter shows average interannual SLA values of −0.95±0.07 cm, −5.98±0.07 cm, −5.06±0.07 cm, 0.58±0.07 cm, 1.08±0.07 cm and 3.87±0.07 cm for NBoB summer season La Niña years of 1998, 1999, 2007, 2010, 2011 and 2016 respectively. LCSCR model also shows similar interannual SLA values of −2.55±0.04 cm, −1.32±0.04 cm, −4.36±0.04 cm, 0.69±0.04 cm, 2.50±0.04 cm and 2.24±0.04 cm for NBoB summer season La Niña years of 1998, 1999, 2007, 2010, 2011 and 2016, respectively. Similar good performance of the LCSCR model also has been observed for CBoB and SBoB regions (Fig. 3). For example, observed data shows average positive interannual SLA values of 7.07±0.07 cm and 2.36±0.05 cm for CBoB and SBoB regions during the summer season La Niña year of 2010.

However, LCSCR shows negative interannual SLA values of -0.59 ± 0.03 cm and -2.25 ± 0.03 cm for the above two regions during the 2010 summer seasons.

The maximum mean absolute deviation of LCSCR in the simulation of the altimeter observed interannual SLA was found during summertime La Niña year of 1999 compared to the other five years (Figure S1). During summertime 1999, the strength of interannual SLA using LCSCR was very weak compared to the altimeter for all three regions (NBoB, CBoB, and SBoB). As an example, the altimeter shows average interannual SLA values of -5.98 ± 0.07 cm, -4.86 ± 0.07 cm and -6.19 ± 0.05 cm for NBoB, CBoB, and SBoB regions, respectively (Fig. 3). However, LCSCR shows average similar negative interannual values of SLA, but with weaker strengths of -1.32 ± 0.04 cm, -0.16 ± 0.03 cm and -2.51 ± 0.03 cm respectively for NBoB, CBoB, and SBoB regions respectively.

It is known from previous research that sea-level variability in the BoB is dominated by the first two modes but for surface current, the role of higher-order modes is prominent (Mukherejee et al. 2017). Similarly, in this article, we found that the two first modes drive sea-level variability in the BoB (Fig. 4). However, the dominance of the vertical mode for interannual SLA variability depends on the density profile used in the LCSCR. The role of the vertical modes on sea-level and surface current variability has been discussed in Mukherejee et al. (2017).

LCSCR model also reasonably well simulates observed interannual variability of SLA along EBoB during the above six summer seasons La Niña years (Fig. 3). As an example, observed strong negative and positive interannual SLA along EBoB during summer season La Niña years of 1999 and 2016 successfully simulated by the LCSCR model. Only during summertime year 1998, LCSCR showed weak positive interannual SLA along EBoB compared to altimeter observed weak negative SLA.

4 Forcing mechanism

In this section, details of linear dynamics related to interannual variability of SLA along WBoB has been discussed using special boundary experiments as described in section 2.

4.1 Role of local and remote forcing

Special boundary experiments on the LCS model showed that observed negative interannual SLA along WBoB during summertime La Niña years of 1998 and 2007 were significantly dominated by remote forcing from EIO (Fig. 5). As an example of the CBoB, LCSCR showed average interannual summertime SLA values of -3.18 ± 0.07 cm and

-6.06 ± 0.07 cm for the years 1998 and 2007, respectively. Four special boundary solutions of the LCS model showed average interannual summertime SLA values of -3.69 ± 0.02 cm, -1.60 ± 0.03 cm, 2.10 ± 0.01 cm and 0.01 ± 0.01 cm using LCS_{EIO}, LCS_{BI}, LCS_{WB} and LCS_{EB} for CBoB regions during La Niña year of 1998 (Fig. 4). Similarly, for the year of 2007, LCS_{EIO}, LCS_{BI}, LCS_{WB} and LCS_{EB} showed average summer interannual SLA values of -5.33 ± 0.02 cm, 0.32 ± 0.03 cm, -0.49 ± 0.01 cm and -0.56 ± 0.01 cm respectively. The dominance of remote EIO forcing was also observed for the NBoB and SBoB regions of WBoB during the summer season for years of 1998 and 2007 (Fig. 5).

Observed negative interannual SLA during summertime La Niña year of 1999 is significantly dominated by destructive interference between remote forcing from EIO and interior BoB (Fig. 5). However, the impact of remote EIO on interannual SLA along WBoB during summertime 1999 is much higher compared to the remote response from interior BoB. As an example along SBoB during summertime 1999, LCSCR showed an average interannual SLA value of -2.51 ± 0.03 cm. Four special boundary solutions of the LCS model showed average interannual SLA values of 2.82 ± 0.02 cm, -7.42 ± 0.03 cm, 1.98 ± 0.01 cm and 0.10 ± 0.01 cm for the LCS_{EIO}, LCS_{BI}, LCS_{WB} and LCS_{EB} respectively for SBoB regions during above summer season year. Similar above dominance of remote interior BoB response has also been observed for the NBoB and CBoB regions during summer of 1999 (Fig. 5).

Using LCS model special boundary experiments, it has been found that positive interannual SLA during the summer season La Niña years of 2010, 2011, and 2016 are significantly dominated by constructive interference between remote forcing from interior BoB and EIO (Fig. 6). Also it has been discussed in section 3 that the best performance of the LCSCR model is restricted in the simulation of observed interannual variability of SLA during summertime years of 2011 and 2016 compared to 2010 (Fig. 3 and section 3). As an example for the NBoB regions during summer seasons, LCSCR shows average interannual values of 0.69 ± 0.03 cm, 2.50 ± 0.03 cm and 2.24 ± 0.03 cm for summertime years of 2010, 2011, and 2016 respectively. LCS_{EIO} shows average interannual SLA values of -1.15 ± 0.03 cm, 1.41 ± 0.03 cm and 0.80 ± 0.03 cm for the NBoB summertime years of 2010, 2011 and 2016 respectively. However, LCS_{BI} shows average interannual SLA values of 2.61 ± 0.03 cm, 1.21 ± 0.03 cm and 1.36 ± 0.03 cm for the summertime years of 2010, 2011 and 2016, respectively. So, constructive interference between remote SLA response from interior BoB and EIO has been observed for the summer seasons of 2011 and 2016 compared to 2010. The contribution of local WBoB wind and remote wind for EBoB is weak and negligible for the above years similar with other La Niña summertime years between 1998–2007.

4.2 Role of equatorial wind

The dominance of EIO remote forcing using LCS_{EIO} has been linked with interannual variability of zonal wind stress along EIO. From January to May of 1998 and 2007, negative zonal wind stress has been observed along EIO, which implies propagation of westward wind direction along EIO (Fig. 7). Westward wind stress along eastern EIO is responsible for generating and propagating upwelling (negative SLA) Kelvin waves along EIO. Equatorial upwelling Kelvin waves generated between January and May of 1998 and 2007 propagated along the eastern boundary of BoB as upwelling Kelvin waves and formed upwelling westward propagating Rossby waves. Above Rossby waves may reach WBoB from the eastern boundary of BoB via central BoB within 3–4 months.

In this study, it has been discussed that interannual variability of SLA are dominated mainly by the first two vertical

modes. As per mode estimation using the LCS model, the speed of the equatorial Kelvin waves for the first mode is $264\,cm\,s^{-1}$. So, the equatorial Kelvin waves may reach the WBoB from eastern EIO within 14–15 days via eastern boundary and northern boundary of the BoB (Mukherjee and Kalita 2019). For the second mode, mode speed reduces to $166\,cm\,s^{-1}$ and will take 25–28 days to reach WBoB from eastern EIO.

The speed of the Rossby waves decreases with an increase in latitude. At 15°N, the speed of the Rossby waves will be $\sim6.2\,cm\,s^{-1}$ for the first mode using LCS model (Mukherjee and Kalita 2019). From 100°E of the eastern boundary to 85°E of the western edge of the BoB, the Rossby waves may take ~3–4 months of time duration to reach. So, the impact of negative zonal wind stress during April in the eastern EIO is expected to be observed during July–August along WBoB. For the second mode, the theoretical speed of the Rossby

Special boundary experiments on interannual SLA (cm)
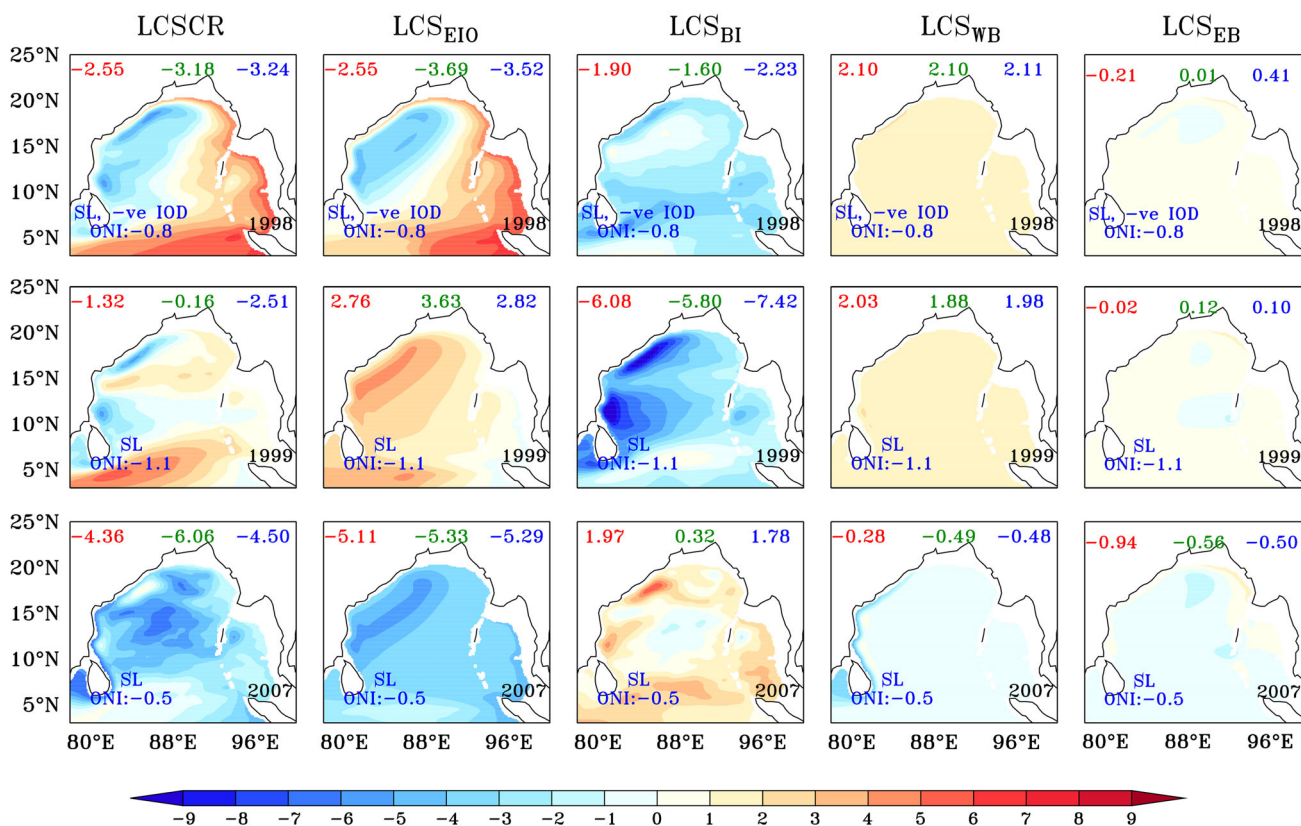
Fig. 5 Forcing mechanism of interannual SLA (cm) for the BoB based on special boundary experiments using LCSCR (as described in Table 1) have been shown here for summertime La Niña years of 1998 (top panel), 1999 (middle panel) and 2007 (bottom panel). Values written in each box using, the red, green, and blue colour represents average values of interannual SLA for NBoB, CBoB, and SBoB regions as showed in Fig. 1. Similar ~400 days low-pass filter has been applied to estimate interannual variability of SLA using LCS_{EIO}, LCS_{BI}, LCS_{WB} and LCS_{EB}

waves will be ~2.5 cm s^{-1} and may take ~6–7 months to reach from the eastern boundary of BoB to WBoB.

So, based on the speed of the Rossy waves, it has been observed that strong positive interannual SLA along WBoB during summer season year of 2011 is linked with solid dominance of positive zonal wind stress between January–May of 2011 in the eastern EIO. Positive zonal wind stress in east EIO forms downwelling (positive SLA) Kelvin waves and propagate along the eastern boundary of the BoB. During propagation of downwelling Kelvin waves along the eastern edge of the BoB, Rossby wave formed as a part of the reflected wave. Then, Rossby waves propagate westward via the central part of BoB and reaches to WBoB within 3–4 months for the first mode and 6–7 months for second mode from the eastern boundary of the BoB as discussed above. So, the impact of positive zonal wind in east EIO during April will be observed during July–August along WBoB for the first mode. Similarly, for the second mode, the impact of favorable zonal wind in the eastern EIO during January will be observed along WBoB during the month of June–August.

4.3 Role of Bay of Bengal wind stress curl

The formation of strong negative interannual SLA along WBoB using LCS$_{BI}$ can be linked with interannual variability of wind stress curl in the BoB (Fig. 8). A statistical correlation has been performed between the interannual variability of wind stress curl in the BoB and interannual SLA (Figure S3). High values of negative correlation have been observed between interannual variability of wind stress curl and interannual SLA using LCS$_{BI}$. A negative correlation is expected because positive (negative) values of wind stress curl in the northern hemisphere will form an upwelling (downwelling) Rossby wave.

The dominance of positive wind stress curl that has been observed during May 1999, in contrast to May 1998 and May 2007, implies the formation of upwelling Rossby waves (negative SLA) in the central BoB (90°E–95°E) due to the counterclockwise rotation of the wind vector. Upwelling Rossby wave formed at the central part of BoB may take 1–2 months to reach WBoB (as per speed of 6.2 cm s^{-1} for the first mode Rossby wave at 15°N using LCS model). Sim-
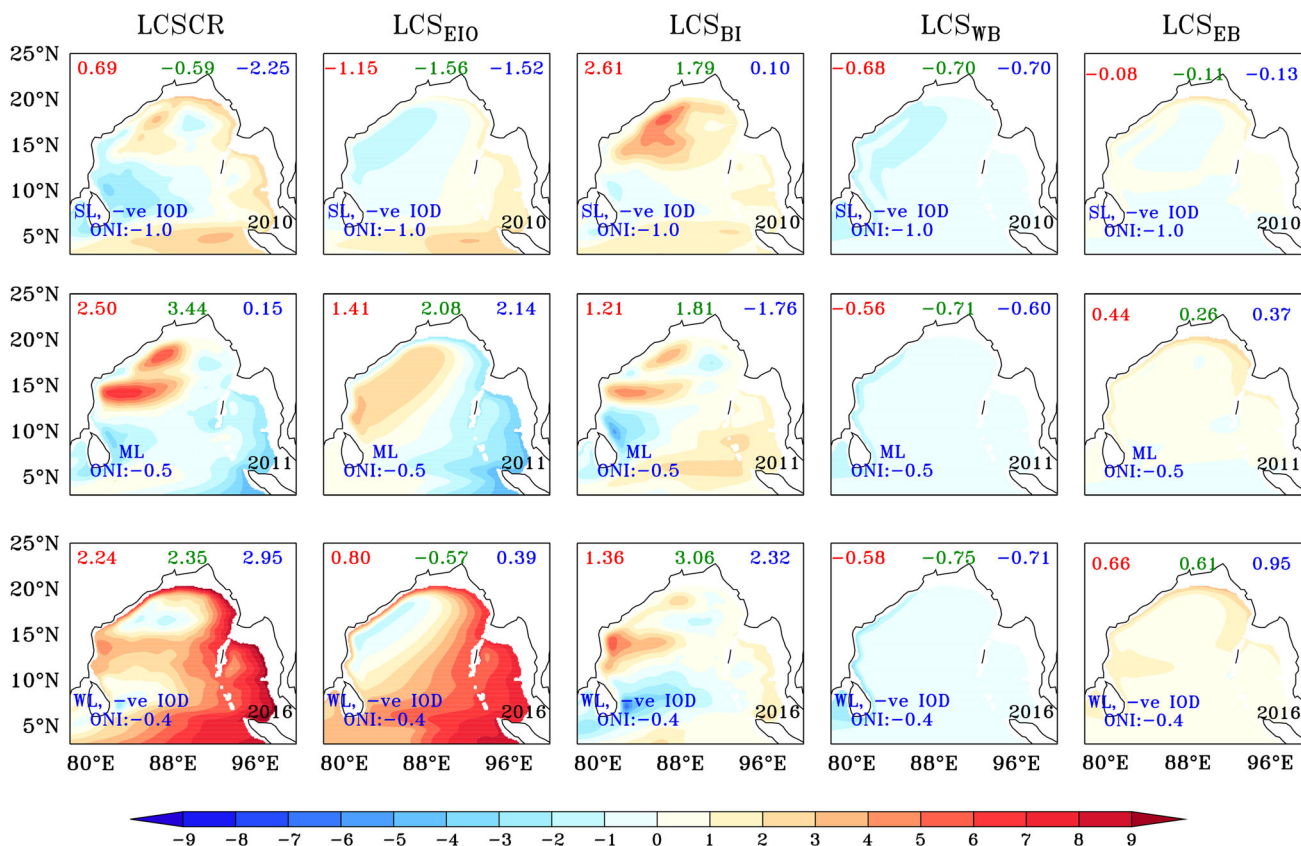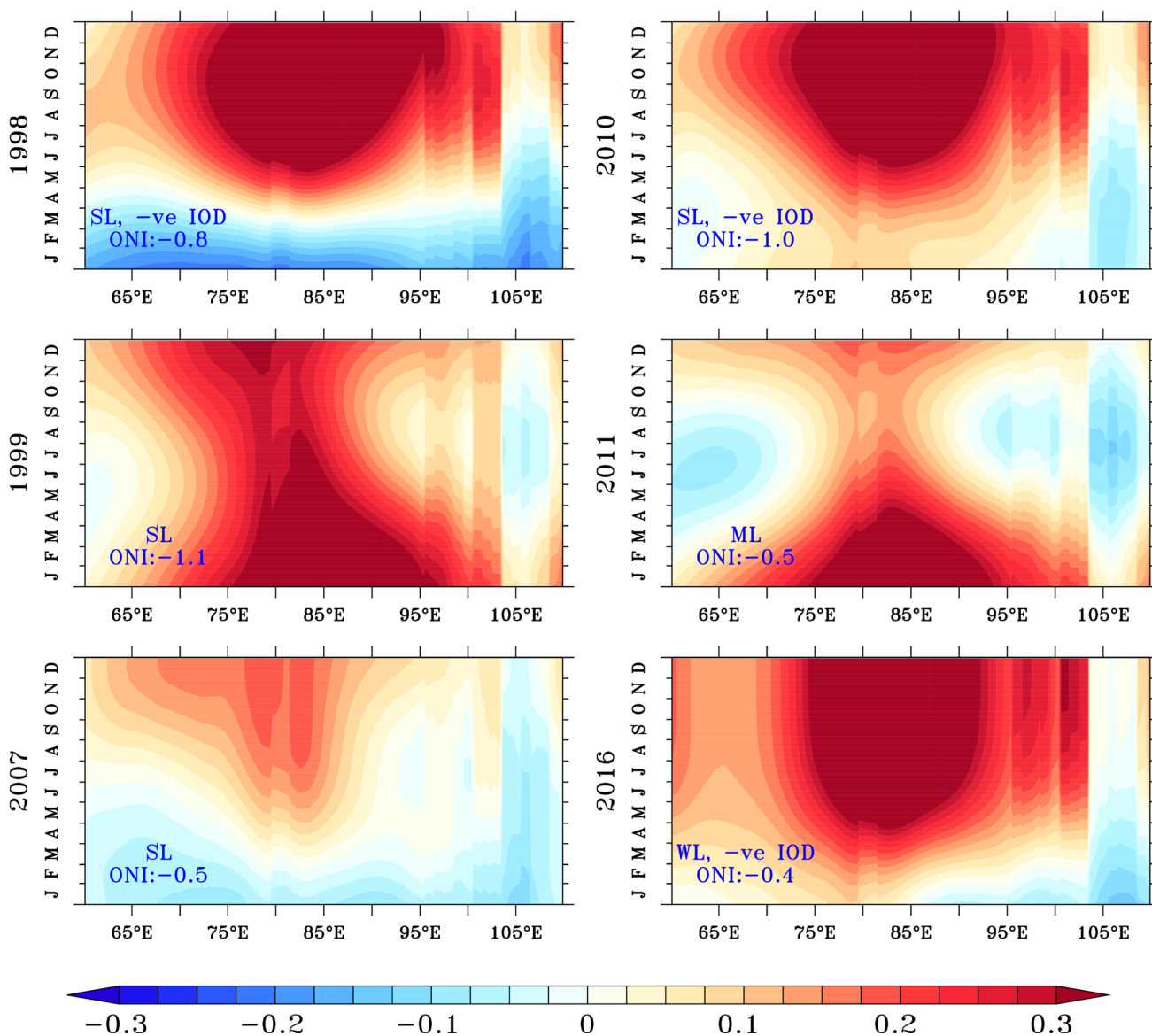

Fig. 6 Similar like Fig. 5, but for the summer season years of 2010, 2011, and 2016

Fig. 7 Interannual variability of equatorial zonal wind stress during La Niña years of 1998, 1999, 2007, 2010, 2011, and 2012. Interannual wind stress (dyne cm^{-2}) data has been averaged between 6.5°N-−6.5°S for estimating equatorial zonal wind stress. The estimation of wind stress using Tropflux (1993–1999), QuikSCAT (2000–2008) and ASCAT (2009–2016) are based on a bulk formula with a drag coefficient from Han and Webster (2002). A similar ~400 days low-pass time series filter has been applied to equatorial zonal wind stress to quantify the interannual variability of zonal wind stress

ilarly, for the second mode, speed of Rossby wave reduces to ~2.5 cm s^{-1} and may take 2–3 months to reach from central BoB to WBoB. So, the impact of the Rossby wave formed at the central part of the BoB (90°E–95°E) during May will be observed during June–July for the first mode and during July-August for the second mode along WBoB.

Positive interannual SLA along WBoB using LCS$_{BI}$ during summer season years of 2010, 2011, and 2016 have been linked with increased negative interannual wind stress curl during the month of May of the above years in the central part of BoB (Fig. 8). As discussed above, increased negative interannual wind stress curl is responsible for the formation of downwelling Rossby (positive SLA) wave via clockwise rotation of wind vector, which may take 1–2 months for the first mode and 2–3 months for second mode to reach WBoB from the central part of the BoB.

Fig. 8 The figure shows BoB interannual wind stress curl (dyne cm^{-3})) during May for the La Niña years of 1998, 1999, 2007, 2010, 2011, and 2016 respectively. The estimation of wind stress using Tropflux (1993–1999), QuikSCAT (2000–2008) and ASCAT (2009–2016) are based bulk formula with drag coefficient from Han and Webster (2002). For estimating interannual variability of wind stress curl, similar ~400 days low-pass time series filter has been applied for both zonal and meridional wind stress. Correlation between interannual variability of wind stress curl and interannual variability of SLA (using an altimeter, LCSCR and LCS$_{EB}$) is shown in Figure S3
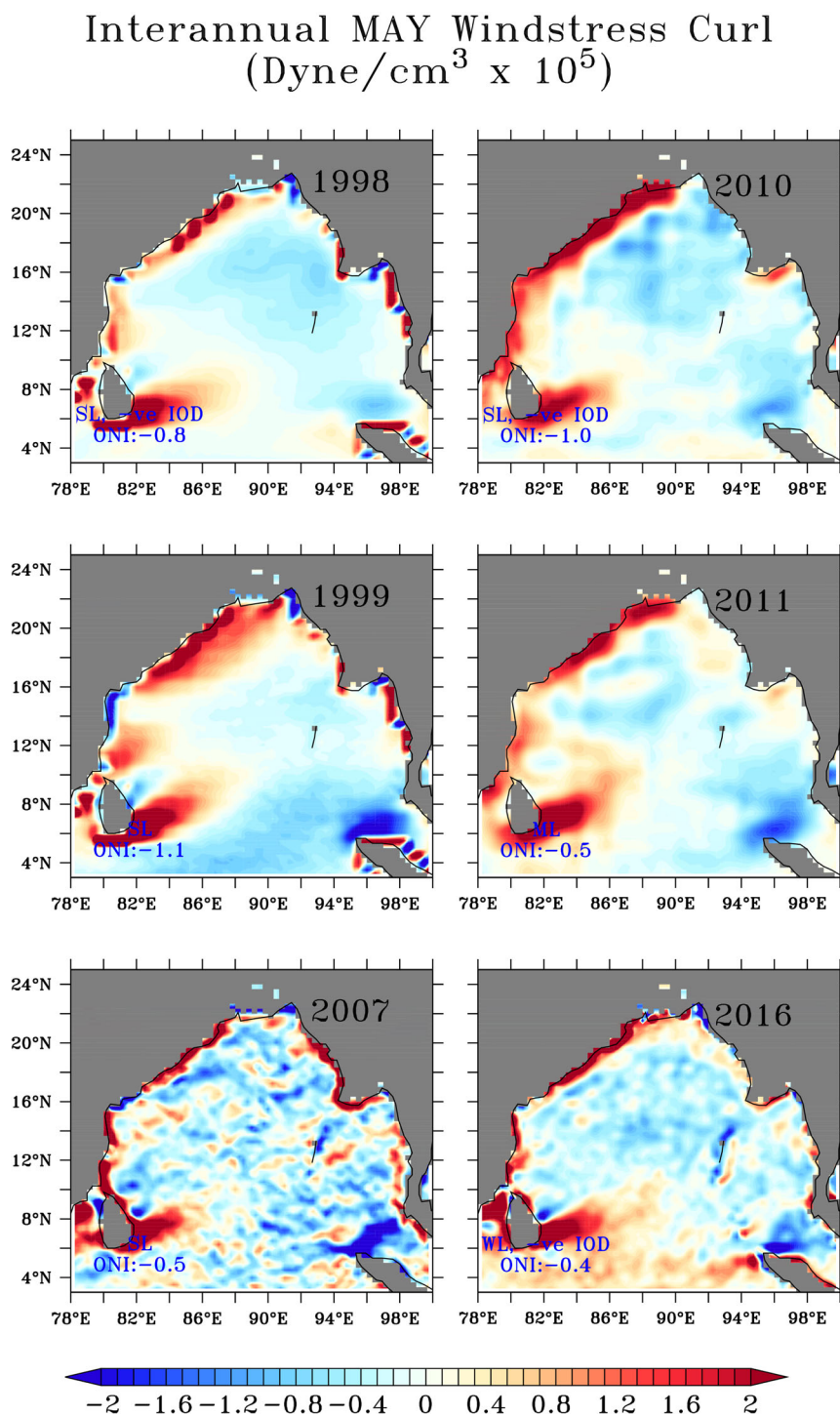
5 Summary and discussions

In this manuscript, interannual changes during the summer seasons along WBoB associated with La Niña events have been discussed using satellite observations and the LCS model. Based on previous research, it was known that during the summer season La Niña years, interannual variability of SLA is weak compared to El Niño year along WBoB (Srinivas et al. 2005; Aparna et al. 2012; Sreenivas et al. 2012). They also showed that during El Niño years, interannual variability of SLA was negative and became positive during La Niña years along WBoB. No study has been performed to know the presence of any dominant interannual variability of SLA associated with La Niña events along WBoB? In this study, using satellite altimeter observations, it has been observed that interannual variability of SLA along WBoB is

not uniform during La Niña years, and it depends on interannual variability associated with remote forcing impact from interior BoB and EIO.

Satellite observations showed negative interannual SLA along WBoB during the summer season La Niña years 1998, 1999, and 2007. However, positive interannual SLA has been observed along WBoB during the summer season La Niña years of 2010, 2011, and 2016. A simple LCS model reasonably well simulates the above observed interannual changes along WBoB during summer seasons La Niña years, but with a slightly weaker magnitude. Using the LCS model special boundary experiments, it has been observed that interannual variability associated with remote forcing from EIO and interior BoB significantly dominates the above interannual changes during summertime La Niña years along WBoB.

Using LCS model special boundary experiments, it has been found that the impact of remote forcing from EIO and interior BoB are not uniform during summertime La Niña years along WBoB. During the summer season La Niña years of 1998 and 2007, interannual SLA along WBoB is negative due to the strong dominance of negative interannual SLA forced by remote EIO wind. However, negative interannual SLA during the summer season La Niña year of 1999 are dominated mainly by negative interannual SLA forced by remote forcing from interior BoB. This implies that negative interannual SLA during the summer season La Niña years of 1998, 1999, and 2007 cannot be explained using remote forcing from EIO only. During the summer season of 1999, positive interannual SLA was observed using remote forcing response from EIO, which was the opposite compared to the summer season of 1998 and 2007. The strong dominance of negative interannual SLA from remote interior BoB compared to positive interannual SLA by remote EIO wind are mainly responsible for negative interannual SLA along WBoB during the summer of 1999.

Negative interannual SLA along WBoB forced by remote EIO wind during summer season La Niña year of 1998 are linked with the dominance of negative zonal wind stress along eastern EIO between January–May of the above years. Similarly, negative interannual SLA along WBoB forced by remote interior BoB during the summer season the year 2007 is linked with a dominance of positive wind stress curl in the central part of BoB compared to other years. So, interannual changes associated with wind stress in the interior BoB and EIO during La Niña years play a major role in interannual changes of SLA along WBoB during the summer seasons.

Using LCS model simulations, it has been observed that positive interannual SLA during recent decade summertime La Niña years of 2010, 2011, and 2016 are dominated mainly by constructive interference between remote response from EIO and interior BoB. Also, during summer seasons of above three years, not much significant changes have been observed associated with interannual variability of zonal wind stress along eastern EIO and wind stress curl in the interior BoB compared to summer seasons La Niña years of 1998, 1999, and 2007.

This manuscript has restricted the detailed discussion of SLA along WBoB during the summer seasons. The changes in La Niña induced interannual variability of SLA during other seasons along WBoB also need to be studied in detail and out of the scope for this manuscript. From this work, it is interesting to note that interannual changes in SLA associated with La Niña events along WBoB need to be studied individually and cannot be predicted based on previous records. More research needs to be performed at BoB to understand interannual changes associated with ENSO events in the coming years. The results also suggest that non-linear effects sometimes become relevant and a more complex model is required to simulate better interannual variability.

Declarations

Conflicts of interest Both authors declare that they have no conflict of interest.

References

Aparna SG, McCreary JP, Shankar D, Vinayachandran PN (2012) Signatures of the Indian Ocean Dipole and EI Nino-Southern Oscillation events in sea level variations in the Bay of Bengal. J Geophys Res 117:C10012. https://doi.org/10.1029/2012JC008055

Chatterjee A, Shankar D, McCreary JP, Vinayachandran PN, Mukherjee A (2017) Dynamics of Andaman Sea circulation and its role in

connecting the equatorial Indian Ocean to the Bay of Bengal. J Geophys Res 122:1–19. https://doi.org/10.1002/2016JC012300

Church JA, White NJ (2011) Sea-Level Rise from the Late 19th to the Early 21st Century. Surveys in Geophysics 32(4–5):585–602. https://doi.org/10.1007/s10712-011-9119-1

Clarke AJ, Liu X (1994) Interannual sea level in the northern and eastern Indian ocean. J Phys Oceanogr 24:1224–1235. https://doi.org/10.1017/1520-0485

Duchon CE (1979) Lanczos filtering in one and two dimensions. J of App Met 18:1016–1022. https://doi.org/10.1175/1520-0450(1979)0183C1016:LFIOAT3E2.0.CO;2

Durand F, Shankar D, Birol F, Shenoi SSC (2009) Spatiotemporal structure of the East India Coastal Current from satellite altimetry. J Geophys Res 114:C02013. https://doi.org/10.1029/2008JC004807

Han W, Webster P (2002) Forcing mechanisms of sea level inter-annual variability in the Bay of Bengal. J Phys Oceanogr 32:216–239. https://doi.org/10.1175/1520-0485(2002)032<0216

Hu A, Bates SC (2018) Internal climate variability and projected futureregional steric and dynamic sea level rise. Nat Commun 9:1068. https://doi.org/10.1038/s41467-018-03474-8

Jensen TG (2007) Wind-driven response of the northern Indian Ocean to climate extremes. J Climate 20:2978–2993. https://doi.org/10.1175/JCLI4150.1

McCreary JP (1980) Modelling wind-driven ocean circulation. Tech. rep., Hawaii Inst. of Geophys

McCreary JP (1981) A linear stratified ocean model of the coastal undercurrent. Phil Trans R Soc Lond A 302:385–413

McCreary JP, Kundu PK, Molinari RL (1993) A numerical investigation of dynamics, thermodynamics and mixed-layer processes in the Indian Ocean. Prog Oceanogr 31:181–244

McCreary JP, Han W, Shankar D, Shetye SR (1996) Dynamics of the East India Coastal Current 2. Numerical solutions. J Geophys Res 101:13993–14010

Moore DW, McCreary JP (1990) Excitation of intermediate frequency equatorial waves at a western ocean boundary: with application to observations from the Indian Ocean. J Geophys Res 95:5219–5231

Mukherejee A, Kalita BK (2019) Signature of La Niña in interannual variations of the East India Coastal Current during spring. Clim Dyn 53:551–568. https://doi.org/10.1007/s00382-018-4601-9

Mukherejee A, Shankar D, Chatterjee A, Vinayachandran PN (2017) Numerical simulation of the observed near-surface East India Coastal Current on the continental slope. Clim Dyn 50:3949–3980. https://doi.org/10.1007/s00382-017-3856-x

Praveen BK, Vialard J, Lengaigne M, Murty VSN, McPhaden MJ, Cronin MF, Pinsard F, Reddy KG (2013) TropFlux wind stress over the tropical oceans: valuation and comparison with other products. Climate Dynamics 40 (7-8)

Rao RR, Girishkumar MS, Ravichandran M, Rao AR, Gopalakrishna VV, Thadathil P (2009) Interannual variability of Kelvin wave propagation in the wave guides of the equatorial Indian Ocean, the coastal Bay of Bengal and the southeastern Arabian Sea during 1993–2006. Deep Sea Res, Part I 57:1–13

Rao S, Behera SK, Masumoto Y, Yamagata T (2002) Inter-annual subsurface variability in the tropical Indian Ocean with a special emphasis on the Indian Ocean Dipole. Deep-Sea Res II 49:1549–1572

Saji NH, Goswami BN, Vinayachandran PN, Yamagata T (1999) A dipole mode in the tropical Indian Ocean. Nature 401:360–363

Schott FA, Xie S, McCreary JP (2009) Indian ocean circulation and climate variability. Rev Geophys 47. https://doi.org/10.1029/2007RG000245

Shankar D, McCreary JP, Han W, Shetye SR (1996) Dynamics of the East India Coastal Current 1. Analytic solutions forced by interior Ekman pumping and local alongshore winds. J Geophys Res 101:13975–13991

Shankar D, Vinayachandran PN, Unnikrishnan AS (2002) The monsoon currents in the north Indian Ocean. Prog Oceanogr 52:63–120

Shankar D, Aparna SG, Mccreary JP, Suresh I, Neetu S, Durand F, Shenoi SSC, Saafani MAA (2010) Minima of interannual sea-level variability in the Indian Ocean. Prog Oceanogr 84:225–241

Shetye SR, Shenoi SSC, Gouveia AD, Michael GS, Sundar D, Nampoothiri G (1991) Wind-driven coastal upwelling along the western boundary of Bay of engal during southwest monsoon. Cont Shelf Res 11:1397–1408

Shetye SR, Gouveia AD, Shankar D, Shenoi SSC, Vinayachandran PN, Sundar D, Michael GS, Nampoothiri G (1996) Hydrography and circulation in the western Bay of Bengal during the northeast monsoon. J Geophys Res 101:14011–14025

Sindhu B, Suresh I, Unnikrishnan AS, Bhatkar NV, Neetu S, Michael GS (2007) Improved bathymetric datasets for the shallow water regions in the Indian Ocean. J Earth syst Sci 116:261–274

Sreenivas P, Gnanaseelan C, Prasad KVSR (2012) Influence of EI Nino and Indian Ocean Dipole on sea level variability in the Bay of Bengal. Glob Planet Change 80–81:215–225. https://doi.org/10.1016/j.gloplacha.2011.11.001

Srinivas K, Kumar PKD, Revichandran C (2005) ENSO signature in the sea level along the coastline of the Indian subcontinent. Indian J Mar Sci 34:225–236

Suresh I, Vialard J, Lengaigne M, Han W, McCreary J, Durand F, Muraleedharan PM (2013) Origins of wind-driven intraseasonal sea level variations in the north Indian Ocean coastal waveguide. Geophys Res Lett 40:5740–5744. https://doi.org/10.1002/2013GL058312